Eur. Phys. J. D **26**, 155–164 (2003)
DOI: 10.1140/epjd/e2003-00208-4

THE EUROPEAN PHYSICAL JOURNAL D

# Experimental study of the $Ca_2$ $^1S+^1S$ asymptote

O. Allard[a], C. Samuelis, A. Pashov[b], H. Knöckel, and E. Tiemann

Institut für Quantenoptik, Universität Hannover, Welfengarten 1, 30167 Hannover, Germany

Received 17 January 2003 / Received in final form 2nd April 2003
Published online 15 July 2003 – 

**Abstract.** The van der Waals coefficients $C_6$, $C_8$ and $C_{10}$ at the $^1S+^1S$ calcium dimer asymptote are determined from spectroscopic observations. The filtered laser excitation technique was applied for measuring transition frequencies of the $Ca_2$ B-X system from asymptotic levels of the $X^1\Sigma_g^+$ ground state reaching $v'' = 38$. That level which is only 0.2 $cm^{-1}$ below the molecular $^1S+^1S$ asymptote has an outer classical turning point of about 20 Å. The extraction of confidence limits for the long range coefficients including the dissociation energy from the experimental data involving Monte Carlo simulation is described. A range for the *s*-wave scattering length is derived.

**PACS.** 31.50.Bc Potential energy surfaces for ground electronic states – 33.20.Kf Visible spectra – 33.20.Vq Vibration-rotation analysis – 33.50.Dq Fluorescence and phosphorescence spectra

## 1 Introduction

In our previous paper [1] we reported on an accurate determination of the $Ca_2$ $X^1\Sigma_g^+$ ground state potential energy curve (PEC) from Laser Induced Fluorescence (LIF) spectroscopy. The study was motivated by the rapid progress in the development of the Ca optical frequency standard [2] and the recent photoassociation spectroscopy data on the $^1S_0+^1P_1$ asymptote [3]. It was considered as the first step of a comprehensive investigation, which should provide a description for short and intermediate internuclear distances of the X state, giving the possibility for further precise determination of the long range part of the PEC from photoassociation spectroscopy or from a molecular beam experiment for example.

The results of the LIF experiments, however, suggested that in the case of $Ca_2$ it might be possible to make a reasonable description of the long range part of PEC already by means of a classical spectroscopy. The potential well of the ground state of $Ca_2$ is so shallow that all rovibrational levels are thermally populated at working temperatures (typically 1220 K), and can be probed by a single laser excitation experiment. Of great importance is also the possibility to extend the description of the PEC by a long range dispersive expansion already from 9.4 Å [1].

For detecting transitions from ground state levels with $v'' > 35$ we applied the Filtered Laser Excitation (FLE) technique, which was used also by Hofmann *et al.* [4] for studying the $A^1\Sigma_u^+$ excited state in $Ca_2$. With this technique we collected spectroscopic information for about 24 highly excited levels of the X state with $v''$ up to 38. The outer classical turning point of the last observed level with $v'' = 38$ and $J'' = 10$ is at 20 Å and is located on the rotationally reduced potential only 0.2 $cm^{-1}$ below the molecular asymptote.

Although the FLE resolution was limited by the Doppler broadening, we will demonstrate that combining the data from [1] and this experiment, it is possible to reduce the uncertainty of the experimentally determined long range coefficients, and especially $C_6$ to an extent, to compare them with the results of the most recent theoretical predictions [5,6].

In Section 2 we explain the experimental set up and discuss the achieved experimental resolution and uncertainties. Section 3 summarizes the methods for constructing of the PEC. Analysis of the experimental data are performed in Section 4, where we employed a Monte Carlo simulation in order to determine the error limits of the fitted long range parameters of the PEC.

## 2 Experiment

The calcium dimers are obtained in a heat pipe oven already described in reference [1]. The experiments are performed with helium or argon buffer gas under a typical pressure of 20–50 mbar and an oven temperature of 1220 K. Working with argon as buffer gas enables us to reduce the pressure to a lower value than with helium without reducing the life time of the heat pipe due to solid calcium closing the optical path. In the frequency

[a] e-mail: allard@iqo.uni-hannover.de
[b] *On leave from* the Institute for Scientific Research in Telecommunications, ul. Hajdushka poliana 8, 1612 Sofia, Bulgaria.

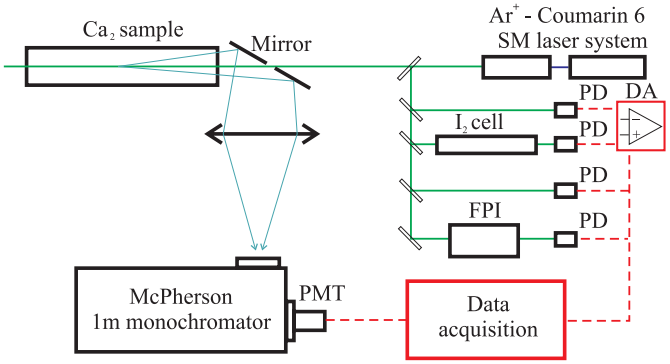


**Fig. 1.** Experimental setup. DA: differential amplifier, FPI: Fabry-Perot interferometer.

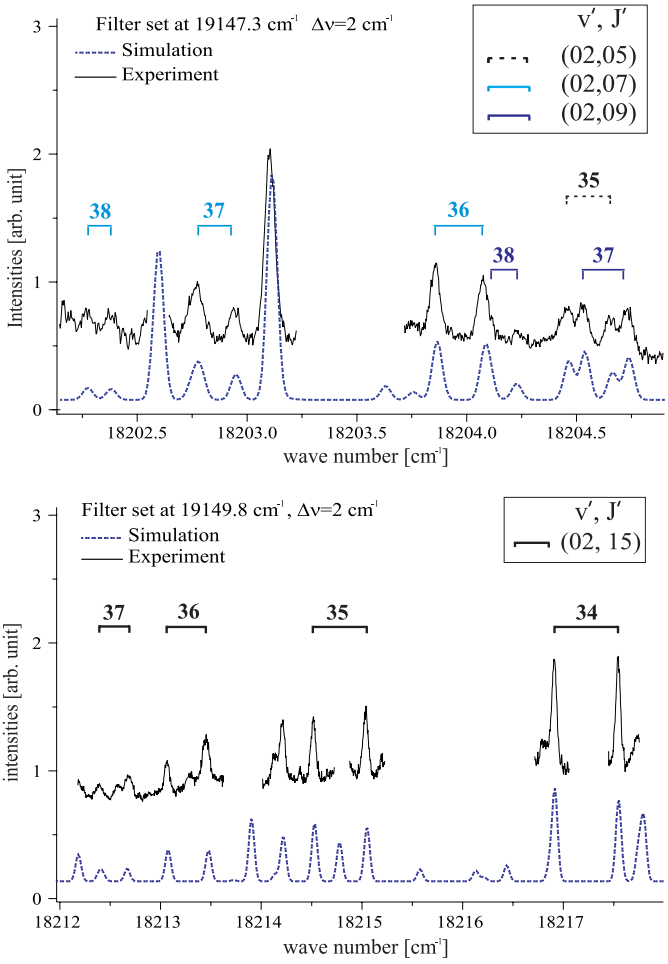


**Fig. 2.** Portions of filtered laser excitation spectra obtained with different detection windows. As dotted lines the synthetic spectra used for assignment of the observed spectral features are shown. Only transitions from ground state levels with $v'' > 34$ are labeled.

range accessible by the lasers in our group the most favorable Franck-Condon factors between the levels close to the asymptote of the $X^1\Sigma_g^+$ state and the levels of the $B^1\Sigma_u^+$ state ($v' = 2$) are less than $10^{-2}$. In order to achieve a sufficient signal-to-noise ratio using Fourier transform spectroscopy a long term stability in the operation of the oven is needed which is not achievable with our present apparatus. In addition, as it was mentioned in reference [1], the discrete fluorescence is accompanied by a strong background emission due to bound-bound-free and free-bound-free molecular transitions. To overcome this problems we chose the filtered laser excitation (FLE) technique for direct excitation of the levels close to the asymptote of the ground state.

A 1 m monochromator (GCA/McPherson Instruments) used as a narrow band pass filter of a typical window width 2 $cm^{-1}$ is set on a strong line of the fluorescence progression when exciting a transition to a selected rotational level with $v' = 2$ of the B state using a single mode dye laser (Coumarine 6). Then the laser operating around 550 nm (60 mW on the $Ca_2$ sample) scans the frequencies of transitions from near asymptote levels of the ground state to the selected $v' = 2$ level. Laser frequencies resonant with such transitions will result in fluorescence, which matches the transmission band of the filter and can be detected. The signal at the output of the monochromator is recorded as a function of the laser wavelength by a photomultiplier (Hamamatsu, R928). Although many other transitions of the X-B system contribute to the absorption spectrum of $Ca_2$ in the scanned spectral region, only excitations which decay into the selected frequency window will be registered. Thus this selective technique provides greatly simplified absorption spectra in a region where the weak transitions from the asymptotic levels of interest are practically completely overlapped by other much stronger transitions.

The relative positions of the FLE lines are calibrated using the frequency comb of a temperature stabilized Fabry-Perot interferometer with a free spectral range of 149.75(1) MHz. The absolute line position is obtained using the absorption spectrum of iodine vapor at room temperature (Fig. 1) calibrated with the IodineSpec calculating software with which the positions of the iodine lines are predicted with an accuracy better than 3 MHz in the studied frequency range [7,8]. In order to improve the signal-to-noise ratio each spectrum is recorded several times. Before the averaging procedure, the recorded signal is normalized to the laser intensity to minimize the influence of its variations with frequency and time. The typical width of the observed lines is 0.05 $cm^{-1}$ corresponding to the Doppler broadening. The intensity of the slowly varying background due to free-bound-free or free-bound-bound transitions of the B-X system is comparable to the intensity of the strongest lines and is mainly responsible for the noise in the spectra. Taking account of the linewidth, the signal-to-noise ratio and the uncertainty in the calibration with the $I_2$ lines, the uncertainty of the absolute frequency for the strongest lines is estimated to be 0.0035 $cm^{-1}$. Two typical spectra are shown in Figure 2 for low and intermediate $J$. The experimental traces as solid lines contain some gaps which were not scanned. The number above the line gives $v''$ and the inset gives $v'$ and $J'$ of the excited state.

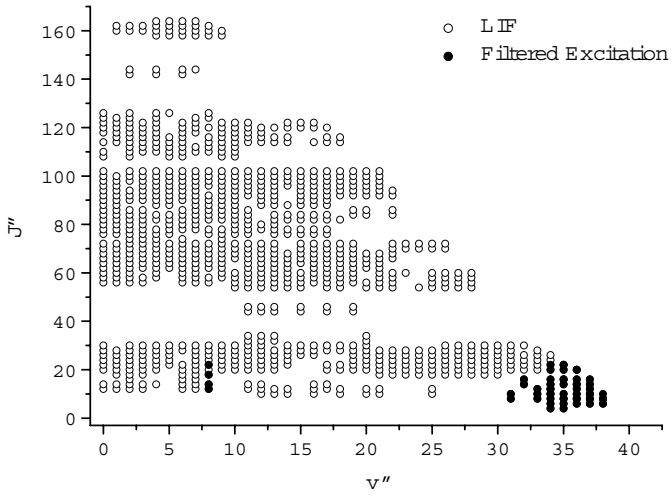


**Fig. 3.** The range of $v''$ and $J''$ quantum numbers of the observed levels in the $X^1\Sigma_g^+$ state of $^{40}Ca_2$.

Using the FLE technique we observed transitions from 44 ground state levels and among them 24 close to the asymptote with $v'' \geq 35$. The last observed levels are ($v'' = 38$, $J'' = 6, 8, 10$) as summarized in the data field in Figure 3. The assignment of the new observed lines is performed using the potential energy curve determined in our previous study of the ground state [1] and a numerical potential of the B state determined from the data available in the literature [9]. Simulations of the transitions by these potentials for selected detection windows are presented in Figure 2 as dotted lines. These lines are shifted vertically with respect to the observed traces in order to show clearly the quality of the simulation. The intensity of the synthetic spectrum is determined by the appropriate Franck-Condon factors, by the thermal population of the ground state levels and by the selected detection window. The small differences between the observed and the simulated spectral features could be attributed to the limited accuracy of the B state PEC (0.05 $cm^{-1}$) and to the fact that the used ground state potential was determined for levels with only $v'' \leq 35$. Also, only transitions in the main calcium isotopomer, $^{40}Ca_2$ were simulated. The unambiguity of the assignment was usually proved further by the observation of relatively long (5-6 vibrational quanta) and self consistent vibrational progressions of P, R doublets.

With the present set-up we can study the influence of the collisions between calcium dimers and the buffer gas by changing its pressure since no additional instrumental broadening on the lines is present. We found that the collisional broadening and the shift of the observed lines are much smaller than what was previously assumed [1]. This means that the experimental uncertainties of the transitions obtained in that study were overestimated.

For completeness we enriched our data with progressions obtained by LIF using the 501.7 nm, 488.0 nm and 457.8 nm lines of an Argon ion laser (Spectra Physics, BeamLok 2060) recorded by Fourier transform spectroscopy. Most of the transitions which are known to be excited by these lines [10] were observed in this study. The present set of transitions representing all the LIF and FLE data covers a range of rotational quantum numbers from $J'' = 4$ to 164 and a range of vibrational quantum numbers from $v'' = 0$ to 38. We have recorded a total of 3580 transitions resulting in 924 levels of the ground state

During this study six atomic calcium lines were also observed around 1.9 $\mu$m, which correspond to the $^3D_{1,2,3} \rightarrow {}^3P_{1,2,3}$ transitions, when irradiating the sample by $Ar^+$ laser lines. These transitions have been already observed in Mg in a similar experiment [11]. Here they could be attributed to predissociation of the molecular B state through a coupling with repulsive states correlated to the $^3D + {}^1S$ asymptotes. It is worth mentioning that the $^3D_{1,2,3} \rightarrow {}^3P_{1,2,3}$ transitions were already observed at temperatures down to 950 K, which suggests that the first step of the process is predominantly excitation of pairs of free Ca atoms by the laser radiation to the molecular B state. The intensity ratio between the infrared emission and the laser light was highest for the 457.8 nm $Ar^+$ line and decreases with the increase of the laser wavelength.

By a new examination of the previous Fourier transform spectra using the new potential energy curve which will be presented in the following, three unassigned weak molecular progressions were found to belong to the calcium isotopomer $^{44}Ca^{40}Ca$. The exciting transitions were identified as $(0, 42) \leftarrow (4, 43)$ and $(0, 72) \leftarrow (5, 73)$ at 18788.36 $cm^{-1}$ and $(0, 111) \leftarrow (8, 112)$ at 18787.36 $cm^{-1}$.

## 3 Construction of PEC

Following the approach adopted in the previous report [1], information which concerns only the ground state was extracted from the raw spectroscopic data. From transition frequencies with a common upper state level, differences between ground state levels were calculated. The PEC for the ground state was then constructed, which describes these experimentally observed differences. Similar to reference [1] the possible combinations of line frequencies within a progression were restricted only to pairs of one P and one R line, forming a total of 8500 differences.

Two different methods for construction of PEC were discussed in detail in reference [1] and will be summarized only briefly here.

The first method represents the potential as a truncated expansion over analytic functions:

$$U(R) = \sum_{i=0}^{n} a_i \left( \frac{R - R_m}{R + bR_m} \right)^i , \qquad (1)$$

where $a_i$, $b$ and $R_m$ are parameters ($R_m$ is close to the equilibrium distance). For short and long internuclear distances the potential is smoothly extended respectively for $R \leq R_{\rm inn}$ with

$$A + B/R^{12} \qquad (2)$$

and for $R \geq R_{\rm out}$ with

$$D_e - C_6/R^6 - C_8/R^8 - C_{10}/R^{10}. \qquad (3)$$

Here $D_e$ is the value of the dissociation energy defined with respect to the minimum of the PEC. Since $R_{out}$ is usually chosen within the region where the contribution of the exchange energy becomes negligible, no additional damping (or cut off) functions for the dispersion coefficients are introduced.

Parameters $a_i$ and $C_6$ and $C_8$ are fitted in a nonlinear fitting procedure (for details see [12]), while $A$, $B$, $C_{10}$ and $D_e$ are adjusted by the program in order to ensure smooth connection between the extensions and the analytic form. $R_m$, $b$ and the connecting points $R_{inn}$ and $R_{out}$ are kept fixed to values, which are experienced from good convergence of the fitting routine.

The second method defines the PEC for short and intermediate internuclear distances as a set of points connected with cubic spline function. For large internuclear distances the same long range expansion as in (3) is used. The values of the potential $U_i$ in a preselected grid of points, $D_e$, $C_6$, $C_8$ and $C_{10}$ are treated as fitting parameters. They are determined in an iterative fitting routine, which linearizes the problem by using a modified version of the inverted perturbation approach [13]. The connecting point $R_{out}$ is chosen in the following way. Initially, the PEC is constructed in a pointwise form up to 13 Å. Then only the long range parameters are fitted assuming that $R_{out} = 9.5$ Å. Although both sections of the PEC are determined independently, their shapes turn out to be almost identical between 9.5 Å and 13 Å. As a last step the $C_{10}$ coefficient of the long range expansion is slightly adjusted (the change does not exceed few percent) in order to fit best the shape of the pointwise potential between 9.4 Å and 10 Å. The crossing point of the pointwise and the long range curves is taken as $R_{out}$. The new value of $R_{out}$ differs from that which was used when fitting the long range parameters. Usually the change is small (typically 0.1 Å) and since the two sections are very close in this region, the effect of such a change on the quality of the fit is negligible. Of course, a second iteration could be performed with the new value of $R_{out}$, but usually it is necessary only in the beginning, when the initial values of the fitting parameters are far from the best ones.

Before fitting the PEC to the new data set, the experimental errors of the data obtained by LIF were reanalyzed, since the value of the normalized standard deviation $\sigma \approx 0.45$ given in the previous study (Ref. [1]) signals their overestimation. The value of the uncertainty before was chosen to be 0.01 cm$^{-1}$ for a strong LIF line in order to take into account possible frequency shifts due to collisions. Since the new FLE measurements showed that the probable influence of the temperature and the buffer gas pressure are much smaller than expected we reduced the errors of all LIF frequencies by a factor of 0.6, which will give a more realistic estimate on the error limits of the fitted PEC parameters.

The analytic potential listed in Table 1 describes the differences between the observed spectral lines from both experiments with a standard deviation $\sigma = 0.0064$ cm$^{-1}$ and normalized standard deviation $\bar{\sigma} = 0.69$. The quality of the PEC for the near asymptotic levels is estimated by calculating the standard deviation with a reduced set of differences, where for each difference at least one level belongs to $v'' \geq 35$. We obtained $\sigma_{35} = 0.0092$ cm$^{-1}$ and $\bar{\sigma}_{35} = 0.92$. The standard deviation for the numerical potential (Tab. 2) are $\sigma = 0.0068$ cm$^{-1}$, $\bar{\sigma} = 0.74$ and $\sigma_{35} = 0.0092$ cm$^{-1}$, $\bar{\sigma}_{35} = 0.89$.

In order to calculate the value of the pointwise potential in the range $R < 9.44$ Å, a natural cubic spline through all the grid points should be used. The parameters of both curves are chosen such, that their minima are set to zero. In order to facilitate the comparison between the dissociation energies $D_0$, defined with respect to the lowest rovibrational level ($v'' = 0, J'' = 0$), their values are given in Tables 1 and 2 as additional parameters.

**Table 1.** Parameters of the analytic representation of the $X^1\Sigma_g^+$ state potential energy curve in $^{40}Ca_2$.

| | |
|---|---|
| $R \leq 3.66$ Å | |
| $R_{inn}$ | 3.66 Å |
| $A$ | $-2.970 \times 10^2$ cm$^{-1}$ |
| $B$ | $7.209 \times 10^9$ cm$^{-1}$Å$^{12}$ |
| 3.66 Å $< R <$ 9.5 Å | |
| $b$ | $-0.5929$ |
| $R_m$ | 4.277277 Å |
| $a_0$ | 0.00043 cm$^{-1}$ |
| $a_1$ | $-2.57153863528197002$ cm$^{-1}$ |
| $a_2$ | $3.79611687289805877 \times 10^3$ cm$^{-1}$ |
| $a_3$ | $3.82947943867555637 \times 10^2$ cm$^{-1}$ |
| $a_4$ | $-2.74470356912936631 \times 10^3$ cm$^{-1}$ |
| $a_5$ | $-3.23378807398046092 \times 10^3$ cm$^{-1}$ |
| $a_6$ | $3.70205119299758223 \times 10^2$ cm$^{-1}$ |
| $a_7$ | $6.35318559107446436 \times 10^3$ cm$^{-1}$ |
| $a_8$ | $-7.39783474312859562 \times 10^3$ cm$^{-1}$ |
| $a_9$ | $-1.90759867971015337 \times 10^4$ cm$^{-1}$ |
| $a_{10}$ | $5.41779135173975228 \times 10^4$ cm$^{-1}$ |
| $a_{11}$ | $4.40527349765557083 \times 10^4$ cm$^{-1}$ |
| $a_{12}$ | $-1.55406021572582802 \times 10^5$ cm$^{-1}$ |
| $a_{13}$ | $-8.35826911941128783 \times 10^4$ cm$^{-1}$ |
| $a_{14}$ | $2.13873243831604603 \times 10^5$ cm$^{-1}$ |
| $a_{15}$ | $1.56022970979522303 \times 10^5$ cm$^{-1}$ |
| $a_{16}$ | $-1.56329579530082468 \times 10^5$ cm$^{-1}$ |
| $a_{17}$ | $-1.46822446075956163 \times 10^5$ cm$^{-1}$ |
| $a_{18}$ | $2.74480910039127666 \times 10^4$ cm$^{-1}$ |
| $a_{19}$ | $7.11882274192053592 \times 10^4$ cm$^{-1}$ |
| $a_{20}$ | $-7.63044568335207146 \times 10^2$ cm$^{-1}$ |
| $R \geq 9.5$ Å | |
| $R_{out}$ | 9.5 Å |
| $D_e$ | 1102.074 cm$^{-1}$ |
| $C_6$ | $1.0030 \times 10^7$ cm$^{-1}$Å$^6$ |
| $C_8$ | $3.87 \times 10^8$ cm$^{-1}$Å$^8$ |
| $C_{10}$ | $4.41 \times 10^9$ cm$^{-1}$Å$^{10}$ |
| Additional parameter | |
| $D_0 = 1069.870$ cm$^{-1}$ | |

**Table 2.** Parameters of the numeric representation of the $X^1\Sigma_g^+$ state potential energy curve in $^{40}Ca_2$.

| $R$ [Å] | $U$ [cm$^{-1}$] | $R$ [Å] | $U$ [cm$^{-1}$] |
|---|---|---|---|
| 3.096980 | 9246.6895 | 5.678571 | 636.3741 |
| 3.188725 | 6566.7325 | 5.809524 | 684.9589 |
| 3.280470 | 4525.7282 | 5.940476 | 728.9235 |
| 3.372215 | 3090.9557 | 6.071429 | 768.5976 |
| 3.463960 | 2134.2175 | 6.202381 | 804.2551 |
| 3.555705 | 1475.2425 | 6.333333 | 836.2419 |
| 3.647450 | 1004.5043 | 6.464286 | 864.8746 |
| 3.739195 | 661.4123 | 6.595238 | 890.4666 |
| 3.830940 | 410.6117 | 6.726191 | 913.2923 |
| 3.922685 | 234.0001 | 6.857143 | 933.6417 |
| 4.014430 | 116.0996 | 6.988095 | 951.7718 |
| 4.106174 | 44.5437 | 7.119048 | 967.8632 |
| 4.197920 | 8.6885 | 7.250000 | 982.2159 |
| 4.289664 | 0.1760 | 7.500000 | 1005.2497 |
| 4.381409 | 11.9571 | 7.750000 | 1023.6698 |
| 4.500000 | 48.5948 | 8.000000 | 1038.3262 |
| 4.630952 | 106.9081 | 8.358974 | 1054.3861 |
| 4.761905 | 175.7311 | 8.717949 | 1066.0579 |
| 4.892857 | 248.8199 | 9.076923 | 1074.5969 |
| 5.023809 | 322.3873 | 9.435897 | 1080.8961 |
| 5.154762 | 393.7222 | 9.794872 | 1085.5974 |
| 5.285714 | 461.4555 | 10.303419 | 1090.2990 |
| 5.416667 | 524.6311 | 10.811966 | 1093.5160 |
| 5.547619 | 582.9870 | 11.611111 | 1096.6870 |
| $D_e = 1102.060$ cm$^{-1}$ | | | |
| $R_{out} = 9.44$ Å | | $C_8 = 3.808 \times 10^8$ cm$^{-1}$Å$^8$ | |
| $C_6 = 1.0023 \times 10^7$ cm$^{-1}$Å$^6$ | | $C_{10} = 5.06 \times 10^9$ cm$^{-1}$Å$^{10}$ | |
| Additional parameter | | | |
| $D_0 = 1069.868$ cm$^{-1}$ | | | |

Comparing the long range parameters from Tables 1 and 2 we can conclude, that using two different representations for the PEC and two different fitting routines we get almost identical values for the dispersion coefficients. It is worth mentioning the differences between the dissociation energies $D_e$ and $D_0$. While the values of $D_0$ agree well within the estimated uncertainty (see the error analysis in Sect. 4), the values of $D_e$ differ significantly. This is due to the uncertainty in the position of the potential minimum $U_{min}$ with respect to the molecular asymptote. In the next section we will estimate this uncertainty and will further refer only to $D_0$, a quantity which is less sensitive to the position of $U_{min}$.

No error bars are attached to the parameters describing the PEC in Tables 1 and 2. An estimate for the uncertainty of the potential for intermediate internuclear distances was presented in reference [1]. By adding the new experimental data we got essentially the same result as shown in Figure 5 of reference [1]. The interpretation of this uncertainty was already discussed in reference [1] and here it will be only stressed that the parameters of the potential in this region have no individual physical meaning. Only the eigenvalues calculated from the total potential will obtain a predictive uncertainty read off from the standard deviations of the fit as given above. The uncertainties of the long range parameters are determined in Section 4 and summarized in Table 3.

**Table 3.** Parameters of the long range expansion for the $X^1\Sigma_g^+$ state in $^{40}Ca_2$ derived in this study and compared with the most recent data from the literature.

| | This study | Other sources |
|---|---|---|
| $D_e$, cm$^{-1}$ | | 1095.0(5) [10] |
| | | 1102.08(9) [1] |
| $D_0$, cm$^{-1}$ | 1069.868(10) | 1069.88(9) [1] |
| $C_6 \times 10^7$ cm$^{-1}$Å$^6$ | 1.003(33) | 1.070(6) [5] |
| | | 1.078 [6] |
| | | 1.15 [10] |
| | | 1.02−1.12 [1] |
| $C_8 \times 10^8$ cm$^{-1}$Å$^8$ | 3.15−4.46 | 3.22 [6] |
| | | 1.1−3.8 [1] |
| $C_{10} \times 10^9$ cm$^{-1}$Å$^{10}$ | 1.7−8.4 | 4.63 [6] |
| | | 3.7−17.0 [1] |

## 4 Uncertainties of the long range parameters

The motivation of this study is not only to describe the rovibrational structure of the $^{40}Ca_2$ ground state. We rather want to examine to which extent the performed spectroscopic study is able to go beyond the reproduction of the observed differences between ground state levels. Of greatest interest is the reliability of the determined long range parameters (and especially $C_6$) since they play an important role in phenomena involving two interacting cold Ca atoms in the ground state.

Our analysis relies on two main assumptions:

- the interaction between two Ca atoms can be described within an adiabatic picture, through a single channel model applying the one dimensional Schrödinger equation with an effective potential energy curve;
- the shape of the potential for internuclear distances $R \geq 9.5$ Å can be described with the long range expression (3), neglecting the exchange energy.

Due to the zero net electronic and nuclear spin in the case of $^{40}Ca$ and the large energy separation between the ground state and the lowest excited states the first assumption seems to be well justified. The second one is supported by the expected small value of the exchange energy [1,14] at 9.5 Å and the dominant van der Waals character of the interaction.

Under these assumptions we ask the question: what are the variations of the PEC parameters around the fitted ones which are still in agreement with the experimental data?

In reference [1] the answer was given with plotting a contour plot of the likehood function $\chi^2$ by varying the

long range parameters. For the nonlinear fitting procedures it is, however, not straightforward how to use the contour plot in order to determine the confidence interval of the parameters since it is not obvious to which confidence limit a given contour corresponds. That is why there is some ambiguity in the probable errors of the fitted parameters determined only by using contour plots. The use of the matrix of variances and covariances, which is obtained by the fitting routines in the linearized form is not useful in our case. The reason is that even if we assume the errors of the experimental frequencies being independent and following a normal distribution, the quantities which enter the fit are actually differences between these frequencies. Consequently, their errors are not independent and we are not allowed to interpret the above mentioned matrix as in the case of independent data points.

A possible way to get the probability distribution of the fitted parameters is to perform a Monte Carlo simulation of synthetic data (see for example [15]).

### 4.1 Monte Carlo simulation

Since our experimental data come with some measurement uncertainties, which we assume to be normally distributed, the set $c^{(0)}$ of the fitted parameters of the PEC will differ from the true one $c^{(t)}$. If we perform a series of similar experiments the experimental data sets will be slightly different and consequently we will obtain different sets of fitted parameters $c^{(\mathrm{exp})}$. Having a sufficient number of measurement sets we could plot the distribution of $c^{(\mathrm{exp})}$ and then decide what are the most probable values and what are their uncertainties.

So let us assume that the fitted potential $U^{(0)}(R)$, described with a set of parameters $c^{(0)}$, is not too far from the true one. Then we can synthesize a set of experimental frequencies which will have exactly the same structure as the one of the present experiment (measurement errors, distribution of $v$ and $J$ quantum numbers). The synthetic frequencies are formed using the eigenvalues for $U^{(0)}(R)$ (since the upper state levels play no role in our analysis, their energies could be set arbitrarily to any value) and adding to each calculated frequency a small random quantity normally distributed with mean value zero and a standard deviation equal to the experimental error. Then we transform the synthetic frequencies into synthetic differences and use the same fitting procedure in order to obtain a new set of parameters $c^{(\mathrm{sim})}$. Performing a large number of simulations we can plot the distribution of $c^{(\mathrm{sim})} - c^{(0)}$. Since the simulated data are related statistically to $U^{(0)}(R)$ in the same way as the existing experimental data to the true potential and since these two potentials were assumed to be close to each other the obtained distribution should be not too different from that of $c^{(\mathrm{exp})} - c^{(t)}$.

For the realization of these ideas we used the pointwise representation of the potential since in the present computer code it allows more flexibility in connecting the long range expansion with the potential curve at intermediate internuclear distances. The price to pay for this is that the first derivative of the PEC might have a small "kink" at $R_{\mathrm{out}}$. This problem, however, does not influence the analysis of the PEC and it could be avoided by slight adjustment of the pointwise curve. What we win is that all the long range parameters are fitted to the experimental data. Since the continuity of the potential is ensured mainly by varying the connecting point $R_{\mathrm{out}}$ and to a smaller extent $C_{10}$ (see the explanation in the previous section), the values of the long range parameters are less influenced by the actual shape of the potential around the connecting point. Analysis similar to those, performed in reference [1] showed that the present body of experimental data fixes very strongly the inner part of the PEC between approximately 3.5 Å and 9.5 Å. Possible variations in this region are connected mainly with the experimental uncertainties and the influence by the selected representation for the potential is negligible. Therefore, we expect that the choice of the connecting point $R_{\mathrm{out}}$ around 9.5 Å makes our analysis almost independent of the functions used to model the PEC at short internuclear distances. On the other hand, possible variation of the inner part may contribute to the uncertainty of the long range coefficients and we take them into account in our analysis.

Having generated a set of synthetic differences $\Delta E^{(\mathrm{sim})}_{v_1J_1,v_2J_2} = E_{v_1J_1} - E_{v_2J_2}$ we treat them as the experimental data. $U^{(0)}(R)$ is taken as initial potential and a small correction to it is fitted which should minimize the difference between $\Delta E^{(\mathrm{sim})}_{v_1J_1,v_2J_2}$ and the differences calculated with the corrected potential. The correction is defined as follows:

$$\delta U(R) = \sum_{i=1}^{N} \delta u_i S_i(R), \text{ for } R < R_{\mathrm{out}} \tag{4}$$

and

$$\delta U(R) = \delta D_e - \frac{\delta C_6}{R^6} - \frac{\delta C_8}{R^8} - \frac{\delta C_{10}}{R^{10}}, \text{ for } R \geq R_{\mathrm{out}}, \tag{5}$$

where $S_i(R)$ are defining functions of the pointwise potential (see [17]), $\delta u_i$ are the values of the correction in an equidistant grid of internuclear distances $R_i$ and $\delta D_e$, $\delta C_6$, $\delta C_8$, $\delta C_{10}$ are the corrections to the long range parameters. Using the theory of perturbations the shift of the difference $\Delta E^{(i)}_{v_1J_1,v_2J_2}$ due to $\delta U(R)$ can be written as:

$$\begin{aligned}\delta(\Delta E^{(i)}_{v_1J_1,v_2J_2}) = &\sum_{i=1}^{N} \delta u_i (K_i^{v_1J_1} - K_i^{v_2J_2}) \\ &+ \delta D_e (L_0^{v_1J_1} - L_0^{v_2J_2}) \\ &- \sum_{j=6,8,10} \delta C_j (L_j^{v_1J_1} - L_j^{v_2J_2}) \,,\end{aligned} \tag{6}$$

where

$$K_i^{vJ} = \int_0^{R_{\mathrm{out}}} \Psi^2_{vJ}(R) S_i(R) \mathrm{d}R \tag{7}$$

$$L_j^{vJ} = \int_{R_{\mathrm{out}}}^{\infty} \Psi^2_{vJ}(R) R^{-j} \mathrm{d}R \tag{8}$$

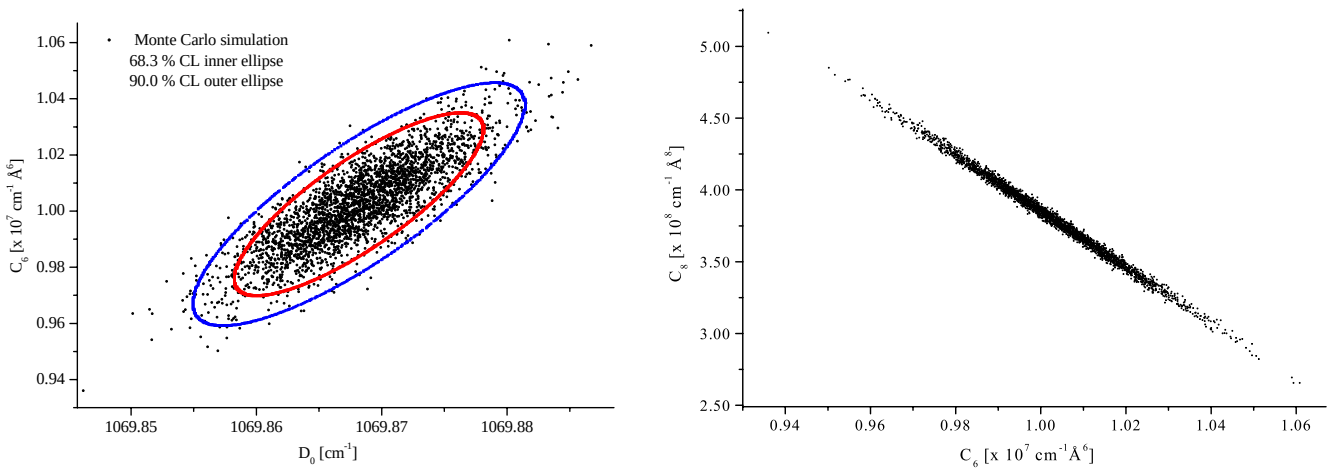


**Fig. 4.** Projections of the long range parameters distribution realized with 3000 simulated points on the $D_0$-$C_6$ and $C_6$-$C_8$ planes. CL stands for confidence limit.

are the corresponding mean values of $S_i(R)$ and $R^{-j}$ calculated with the wave functions $\Psi_{vJ}(R)$ of the levels forming the difference.

Note that in principle the exact representation of $U^{(0)}(R)$ is not of importance since we study only the possible small variations around it which are allowed by the error intervals of the experimental data. The advantage of expressing the correction to the potential in a pointwise form (cubic spline function is used for interpolation) is that the influence of the parameters $\delta u_i$ is localized in $R$, since away from $R_i$ $S_i(R)$ decays exponentially [13]. This gives a high flexibility in constructing the needed form of the correction. Additionally, the correlations between $\delta u_i$ are introduced mainly by the experimental data and not by the selected basis functions $S_i(R)$.

With each set of simulated data a new fit is performed which adjusts $\delta u_i$, $\delta D_e$, $\delta C_6$, $\delta C_8$ and $\delta C_{10}$. Along with this we examine the contributions (the sums in Eq. (6)) due to $\delta u_i$ and the long range corrections to the fitted differences. As it could be expected, the changes of the PEC for $R < R_{\rm out}$ are very small ($\delta u_i \sim 0.01$ cm$^{-1}$) for all sets of synthetic data due to the large amount of experimental observations in this region. In addition the corrections to the differences due to $\delta u_i$, *i.e.* the first term of the right side of equation (6), turn out to be smaller than the corresponding experimental uncertainties and in principle one could neglect them. We checked this and, indeed, the distribution of the long range parameters was almost identical for simulations with and without fitting $\delta u_i$. Since this is true for different numbers of $\delta u_i$ parameters, we may consider it as a proof of the statement made above, that in the present case the determination of the long range parameters is almost independent on the model used to describe the inner part of the PEC.

The positions of the energy levels and the molecular asymptote $D_e$ in reference [1] were defined with respect to the minimum of the PEC, $U_{\rm min}$. Then we estimated that the possible variation of $U_{\rm min}$ for different representations of the potential is of the order of 0.01 cm$^{-1}$, which was smaller than the uncertainty of the dissociation energy, 0.09 cm$^{-1}$. With the extended experimental data set and after the revision of the earlier experimental uncertainties we are now able to give a much better prediction of the dissociation energy with uncertainty also of the order of 0.01 cm$^{-1}$. Obviously defining the dissociation energy with respect to $U_{\rm min}$ will introduce an undesired increase of the uncertainty for this quantity. Consequently, from here on we will consider only the value of the dissociation energy $D_0$ defined with respect to the lowest rovibrational level $E_{00} = E_{v''=0,J''=0}$. Indeed, fitting $\delta u_i$ to the simulated data we convinced ourselves that although the shape of the potential (and also $U_{\rm min}$) will vary slightly from fit to fit, the overall effect on the position of $E_{00}$ is much smaller than the typical variation of $U_{\rm min}$. Nevertheless, the contribution of $E_{00}$ to the uncertainty of $D_0$ is taken into account.

In this way, the main steps of the performed Monte Carlo analysis are:

1. find the PEC $U^{(0)}(R)$ which can reproduce the experimental observations with smallest standard deviation;
2. from the eigenvalues for $U^{(0)}(R)$ generate a set of synthetic data by adding normally distributed random deviations according the experimental uncertainties. This set has exactly the same structure as the experimental data;
3. perform a fit with the synthetic data as it was done with the original one and collect the obtained potential parameters in a distribution list;
4. repeat steps (2–4) until enough simulated long range parameters are collected in order to analyze their distribution.

### 4.2 Results

In Figure 4 two projections of the long range parameters distribution obtained from 3000 simulations are shown. It is worth mentioning the strong correlation between $C_6$ and $C_8$, which is the case also for the other pairs of dispersive coefficients.

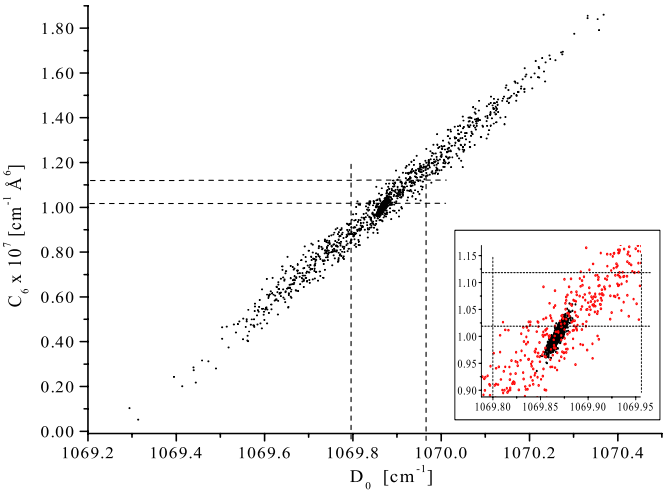


**Fig. 5.** Projections of the long range parameters distributions on the $D_0$-$C_6$ plane derived from the LIF data from reference [1] and from the present study (the black spot in the centre). The horizontal dotted lines denote the uncertainty of $C_6$ assumed in reference [1] and the vertical ones the probable variation of $D_0$.

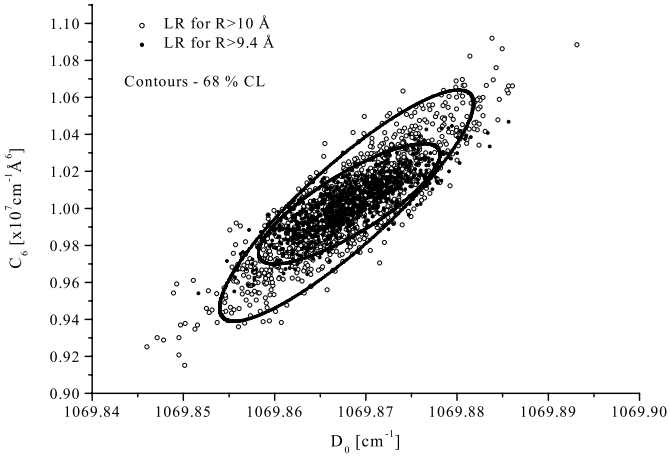


**Fig. 6.** Projections of the long range parameters distributions on the $D_0$-$C_6$ plane derived by assuming the validity of the long range expansion from 9.4 Å (solid circles) and from 10 Å (open circles).

In order to determine the confidence regions for the parameters we construct an ellipsoid in the four dimensional space of the parameters, whose axes have such orientations and relative lengths that the resulting surface follows the form of the distribution. Then we change gradually the lengths of the axes by a constant factor and count the number of points which are enclosed by the ellipsoid. For example, the ellipsoid which contains 68.3% of the points will determine the 68.3% ($1\sigma$) confidence region of the parameters. The projections of the 68.3% and the 90% confidence regions (strictly speaking the contours surrounding the projections) are plotted as ellipses in the left part of Figure 4 for the pair of parameters $D_0$ and $C_6$.

This allows us to determine the mean value and uncertainty of the dissociation energy of the $^{40}Ca_2$ ground state with respect to the lowest rovibrational level as $1069.868 \pm 0.010\,\mathrm{cm}^{-1}$ and of the $C_6$ coefficient as $(1.003 \pm 0.033) \times 10^7\ \mathrm{cm}^{-1}\text{Å}^6$ at a confidence limit of 68.3%. The values and the uncertainties of all the long range parameters are summarized in Table 3 and compared with the values from other sources.

The highest observed rovibrational level in reference [1] had $v'' = 35$ and it was concluded that with the available experimental data set it is not possible to give any reasonable estimation for $C_6$. Now, by using a Monte Carlo analysis we can be more rigorous. In Figure 5 we compare the projections of two distributions on the $D_0$-$C_6$ plane. The broader one is derived using only the data from reference [1] before the revision of those experimental errors. In order to obtain a meaningful estimation of the dissociation energy of the X state, we restricted in reference [1] the possible variation of $C_6$ within a $\pm$ 5% interval around the theoretical value [5]. This interval is denoted in Figure 5 with horizontal dashed lines. The uncertainty of the dissociation energy can be determined by projecting the distribution within this interval on the $D_0$ axis and we get a similar uncertainty like in reference [1]. After including the new LIF and FLE data the distribution shrinks to the small black spot in the centre of Figure 5 (see also the inset), which is actually the distribution from Figure 4. It would be, however, not correct to interpret the drastic reduction of the size of the distribution only as a result of the transitions involving rovibrational levels with $v'' > 35$. In fact the items, which led to the distribution presented in Figure 4 are:

- the assumption that the long range expansion (3) is valid starting from 9.5 Å. This allows to link the values of the long range parameters with the frequency differences involving levels with $30 \leq v'' \leq 38$, *i.e.* the shape of the long range potential is roughly tested from 9.5 Å up to $\approx$ 20 Å (the classical turning point of the last observed level). A Monte Carlo simulation shows (Fig. 6) the change of the distribution when shifting $R_{\mathrm{out}}$ from 9.4 Å only by 0.6 Å to $R_{\mathrm{out}} = 10$ Å. Note, that in this case the loss of accuracy on $C_6$ is larger by a factor of two compared to the increase of the $D_0$ uncertainty;
- availability of highly excited levels with $v'' = 38$, since they limit the variation of the dissociation energy;
- the enlargement of the experimental data, which allow accurate determination of the PEC for short and intermediate internuclear distances. Because of the large body of data, the long range parameters are almost independent of the exact representation of the rest part of the PEC, which is clearly indicated by the small variations of $\delta u_i$ (Eq. (6)) during the statistical analysis;
- the corrected estimate of the experimental uncertainties of the data in reference [1].

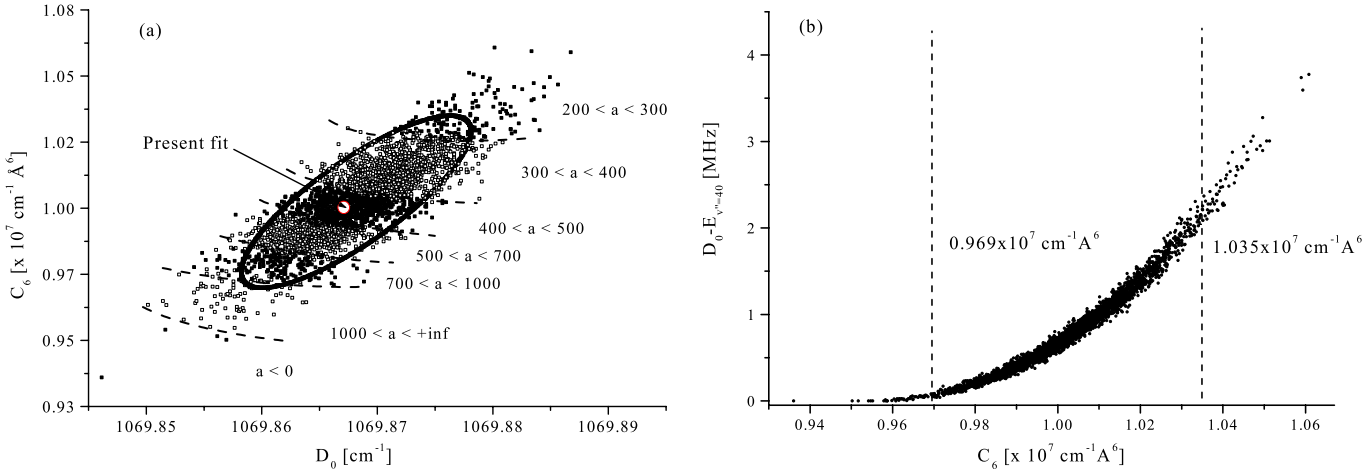


**Fig. 7.** (a) Relation of $C_6$-$D_0$ distribution with the $s$-wave scattering length $a$, and (b) the distribution of the position of the last bound level with respect to the asymptote for the long range potentials obtained from the Monte Carlo simulation.

### 4.3 The value of the $C_6$ coefficient

The 68.3% confidence interval for $C_6$ given in this paper $(1.003 \pm 0.033) \times 10^7$ cm$^{-1}$Å$^6$ does not overlap with the most recent theoretical prediction of $(1.070 \pm 0.006) \times 10^7$ cm$^{-1}$Å$^6$ within the error stated in reference [5].

From our side, we realize that an important point in our analysis is the assumption for the validity of the long range expansion (3) down to $\approx 9.5$ Å. As it was shown in Figure 6, shifting $R_{\rm out}$ to larger internuclear distances will increase the uncertainty on the fitted parameters. The same will happen if we introduce additional terms into the long range model (for example the exchange energy). Our analysis can readily include these additional parameters, provided there are new experimental observations which require this. In general, however, since the exchange term is repulsive for the $^1S+^1S$ asymptote, the value of $C_6$ obtained here is expected to be an effective one which includes the exchange contribution and which is thus smaller than the so called true one.

In order to estimate the possible influence of the exchange energy, we added to the long rang model (3) an exchange term $E_{\rm exch}(R) = AR^\alpha \exp(-\gamma R)$. The values for $A$, $\alpha$ and $\gamma$ were kept fixed at the theoretical values taken from [14,16]. The fitting procedure described in Section 3 in this case led, as expected, to a somewhat higher value of $C_6 = 1.034 \times 10^7$ cm$^{-1}$Å$^6$ and $D_0 = 1069.873\,$cm$^{-1}$. The quality of the fit did not change. The distribution of the long range parameters remains the same as before taking into account the exchange energy, but centered around the new values.

### 4.4 The s-wave scattering length

In order to obtain the $s$-wave scattering length and its confidence interval, it is straightforward to calculate its value for each of the simulated PEC. These calculations will show how reliably the spectroscopically determined potential up to $\approx 20$ Å can be applied to model cold collisions. The results are presented in Figure 7a. The position of the last bound level ($v'' = 40$) with respect to the molecular asymptote, $D_0 - E_{v''=40,J''=0}$ is shown in Figure 7b. The values of the scattering length $a$ within the 68.3% confidence region vary from $250a_0$ to $1000a_0$ (Bohr radius $a_0 \approx 0.52918$ Å). Since these values indicate a bound level very close to the asymptote (several MHz, see Fig. 7b), initially we were surprised that from our much less accurate data (several 100 MHz) we can make such a good prediction of the position of the last bound level. Obviously, the large amount of observed data fixes the accumulated phase of the wave function for this level along the PEC up to $\approx 20$ Å and the variation of the binding energy with respect to the asymptote is restricted mainly by the uncertainty of $C_6$. In addition, from Figure 7b we see that the smaller the binding energy, the less sensitive it is to the uncertainties of the other long range parameters.

The inner wall of the potential ($R < 3.5$ Å), however, is not well fixed by the experimental data. Could its change shift the last level by several MHz without influencing the positions of the other levels? The answer is negative. The wave functions for small internuclear distances for the highly excited levels differ only by a constant factor. For example, for a PEC with binding energy $D_0 - E_{40} \approx 3$ MHz for $v'' = 40$, the shapes of the wave functions for $v'' = 40$ and $v'' = 35$ are almost identical up to 7.5 Å and the ratio between them is:

$$\frac{\Psi_{v''=35}(R)}{\Psi_{v''=40}(R)} \approx 35 \text{ for } R < 7.5 \text{ Å}. \qquad (9)$$

So, using the perturbation theory it is clear, that a change of the potential for $R < 3.5$ Å, which will shift the position of the level with $v'' = 40$ by 1 MHz will shift the level with $v'' = 35$ by $\approx 1.2$ GHz (0.04 cm$^{-1}$). Since this change will not alter for example the position of the lowest level ($v'' = 0$), the introduced shift of the difference $E_{v''=35} - E_{v''=0}$ will exceed the experimental uncertainty roughly by a factor of 6, which is a contradiction.

Due to the revised confidence interval for the $C_6$, the uncertainty of the scattering length was not reduced compared to reference [1] ($112a_0 \div 800a_0$), although the uncertainty of $C_6$ itself is smaller than the assumed one in reference [1] ($\pm 5\%$ around the theoretical prediction of $1.07 \times 10^7$ cm$^{-1}$Å$^6$ [5]). Following the dependence of the binding energy on the last level on $C_6$ (Fig. 7b) we see that for smaller values of $C_6$ this level approaches the asymptote, which makes an accurate determination of the scattering length more difficult.

The discussion in the previous section showed, that by neglecting the exchange energy, the fitted value of $C_6$ could be considered as determining the lower possible limit for this parameter. If the increase of $C_6$ would not exceed the expected few percent, this can lead to a shift of the possible magnitude of the scattering length to smaller, but still positive values (see Fig. 7a). For example, with the theoretical parameters for the exchange energy from [14] and [16] we get $C_6 = 1.034 \times 10^7$ cm$^{-1}$Å$^6$ and an interval for the scattering length $200a_0 \div 800a_0$,

## 5 Conclusions

The $^1$S+$^1$S molecular asymptote of the Ca dimer was studied by employing the filtered laser excitation technique. The spectroscopic data obtained in our previous study by Fourier transform spectroscopy were enriched by adding 56 transition frequencies from ground state levels with $v''$ up to 38. This gave us an opportunity to reanalyze the existing description of the long range part of the PEC from reference [1].

By assuming the long range expansion (3) for the potential energy curve to be valid already from 9.5 Å, the probability distributions of the dissociation energy and the dispersion coefficients were derived from Monte Carlo analysis. Their mean values and uncertainties are given in Table 3. We showed, that due to the large amount of experimental data, the long range analysis is almost independent of the model functions used to describe the inner part of the PEC.

The reliability of the experimental potential for describing collisions between two Ca atoms at low temperatures was checked by calculating the $s$-wave scattering length and the position of the last bound level with respect to the asymptote for the variety of long range extensions of the potential allowed by the present experimental data. Following the distribution of the long range parameters, the binding energy of the last level was found to vary between several 10 kHz and several MHz. This confirmed our anticipations [1] for a large and positive scattering length, $250a_0 < a < 1000a_0$. Contrary to the previous study, the present determination is purely experimental and does not rely on the theoretical estimations for $C_6$. The difference in the values of $C_6$ from reference [5] and from this study exceeds the stated uncertainties, although a small model dependence is still existing by neglecting the exchange energy and by altering the connecting point between the inner potential and the long range branch (compare Fig. 6).

The Monte Carlo simulations open good perspectives for analyzing the uncertainties of the parameters of the PEC. They could be used also to determine the kind of spectroscopic data and their required accuracy for achieving the desired uncertainty of the fitted parameters. For example, we checked that including a vibrational progression up to $v'' = 39$ with the present experimental accuracy will not reduce the uncertainties of $C_6$ and $D_0$ significantly. This could be reached, however, even with the present distribution of data, provided the accuracy can be improved. Therefore, we believe that only high resolution Doppler free spectroscopic techniques should be used for further improvement on the $Ca_2$ ground state PEC, especially at long internuclear distances.

This work is supported by DFG through SFB 407. The authors appreciate the assistance of St. Falke during the experiments. A.P. gratefully acknowledges the research stipend from the Alexander von Humboldt Foundation.

## References

1. O. Allard, A. Pashov, H. Knöckel, E. Tiemann, Phys. Rev. A **66**, 042503 (2002)
2. G. Wilpers, T. Binnewies, C. Degenhardt, U. Sterr, J. Helmcke, F. Riehle, Phys. Rev. Lett. **89**, 230801 (2002)
3. G. Zinner, T. Binnewies, F. Riehle, E. Tiemann, Phys. Rev. Lett. **85**, 2292 (2000)
4. R.T. Hofmann, D.O. Harris, J. Chem. Phys. **85**, 3749 (1986)
5. S. Porsev, A. Derevianko, Phys. Rev. A **65**, 020701(R) (2002)
6. R. Moszynski, private communication, 2001
7. IodineSpec can be found on the web site `www.toptica.com`
8. H. Knöckel, E. Tiemann, private communication
9. W.J. Balfour, R.F. Whitlock, Can. J. Phys. **53**, 472 (1975)
10. C.R. Vidal, J. Chem. Phys. **72**, 1864 (1980)
11. H. Scheingraber, C. Vidal, J. Chem. Phys. **66**, 3694 (1977)
12. C. Samuelis, E. Tiesinga, T. Laue, M. Elbs, H. Knöckel, E. Tiemann, Phys. Rev. A **63**, 012710 (2000)
13. A. Pashov, W. Jastrzębski, P. Kowalczyk, Comput. Phys. Commun. **128**, 622 (2000)
14. A.A. Radzig, P.M. Smirnov, *Reference Data on Atoms, Molecules and Ions* (Springer, Berlin, 1985)
15. T.-S. Ho, H. Rabitz, G. Scoles, J. Chem. Phys. **112**, 6218 (2000)
16. A. Kleinekathofer *et al.*, J. Chem. Phys. **103**, 6617 (1995)
17. A. Pashov, Ph.D. thesis, Institute of Physics, Polish Academy of Sciences, Warsaw, 2000